A high-valent non-heme μ-oxo manganese(IV) dimer generated from a thiolate-bound manganese(II) complex and dioxygen

Déborah Brazzolotto, Fabián G. Cantú reinhard, Julian Smith-Jones, Marius Retegan, Lucia Amidani, Abayomi S. Faponle, Kallol Ray, Christian Philouze, Sam P. de Visser, Marcello Gennari, et al.

HHS Public Access

Author manuscript

Angew Chem Int Ed Engl. Author manuscript; available in PMC 2018 July 03.

Published in final edited form as:

Angew Chem Int Ed Engl. 2017 July 03; 56(28): 8211–8215. doi:10.1002/anie.201703215.

A high-valent non heme μ-oxo Mn^{IV} dimer generated from a thiolate-bound Mn^{II} complex and O_2

Dr. Deborah Brazzolotto[a],[b], **Fabián G. Cantú Reinhard**[c], **Julian Smith-Jones**[a], **Dr. Marius Retegan**[d], **Dr. Lucia Amidani**[d], **Dr. Abayomi S. Faponle**[c], **Prof. Kallol Ray**[e], **Dr. Christian Philouze**[a], **Dr. Sam P. de Visser**[c], **Dr. Marcello Gennari**[a], and **Dr. Carole Duboc**[a]

[a]Univ. Grenoble Alpes, CNRS, UMR 5250, DCM, F-38000 Grenoble, France

[b]Univ. Grenoble Alpes, CNRS, UMR 5249, LCBM, F-38000 Grenoble, France

[c]Manchester Institute of Biotechnology and School of Chemical, Engineering and Analytical Science, The University of Manchester, 131 Princess Street, Manchester M1 7DN, United Kingdom

[d]European Synchrotron Radiation Facility (ESRF), 71 Avenue des Martyrs, 38000, Grenoble, France

[e]Department of Chemistry,Humboldt-Universität zu Berlin Brook-Taylor-Strasse2,12489 Berlin (Germany)

Abstract

This study deals with the unprecedented reactivity of dinuclear non heme Mn^{II}–thiolate complexes with O_2, which dependent on the protonation state of the initial Mn^{II} dimer selectively generates either a di-μ-oxo or μ-oxo-μ-hydroxo Mn^{IV} complex. Both dimers have been characterized by different techniques including single-crystal X-ray diffraction and mass spectrometry. Oxygenation reactions carried out with labeled $^{18}O_2$ unambiguously shows that the oxygen atoms present in the Mn^{IV} dimers originate from O_2. Based on experimental observations and DFT calculations, evidence is provided that these Mn^{IV} species comproportionate with a Mn^{II} precursor to yield μ-oxo and/or μ-hydroxo Mn^{III} dimers. Our work highlights the delicate balance of reaction conditions to control the synthesis of non heme high-valent μ-oxo and μ-hydroxo Mn species from Mn^{II} precursors and O_2.

Graphical Abstract

Thiolate is the key. Dinuclear Mn^{II}–thiolate complexes display an unprecedented reactivity: direct O_2 activation to generate dinuclear high-valent oxo Mn species, including a di-μ-oxo Mn(IV) dimer. Depending on the experimental conditions, the nature of the oxidized Mn species is different. A mechanism based on theoretical calculations is discussed to rationalize all experimental data.

Correspondence to: Sam P. de Visser; Marcello Gennari; Carole Duboc.

Supporting information for this article is given via a link at the end of the document.

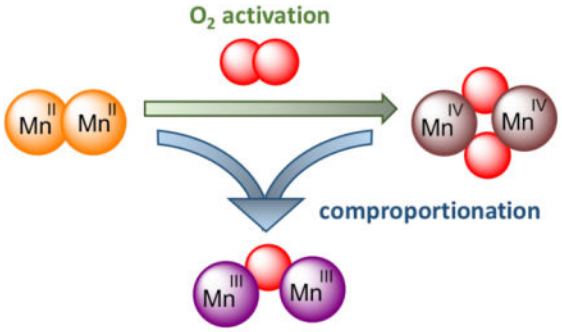

Keywords

O_2 activation; manganese; thiolate; high valent oxo species; mechanistic studies

Dioxygen activation is critical for all forms of life and fundamental in many biological processes.[1] In addition, O_2 is an environmentally benign oxidant in chemical catalysis[2] and the development of fuel cells requires electrocatalysts for its efficient and selective reductive activation.[3] Activating O_2 often requires transition metal ions to promote the process.[4] The detailed understanding of the role of the metal ion and of the mechanism at a molecular level, especially through the characterization of intermediate species, is therefore crucial for the development of efficient catalysts.[5] Surprisingly, even though mono- and dinuclear high-valent metal oxo species derived from O_2 have been extensively described for iron[6] and copper,[7] little is known on the dioxygen chemistry of manganese,[8] another cheap and abundant metal. In particular, a non heme oxo Mn^{IV} complex *directly* generated by reacting O_2 with a Mn^{II} precursor has yet to be described. Mononuclear oxo and dinuclear μ-oxo Mn^{IV} complexes have been quasi-exclusively generated using oxidizing agents such as H_2O_2, PhIO or peracids.[8–9] There is only one case reported by Borovik et al in which the synthesis of an oxo-Mn^{IV} complex derived from O_2 and a Mn^{II} precursor has been described, but the presence of ferrocenium was required to oxidize the intermediate Mn^{III} species.[10] In a few other studies, oxo-Mn^{IV} species derived from O_2 and a Mn^{II} complex have been suggested as intermediates but without direct experimental evidence.[11] Recently, McKenzie et al evoked the formation of such transient species during the oxidation of benzylic C-H bonds by a Mn^{II} complex with O_2.[11a] Kovacs et al reported that Mn^{II} complexes with a thiolate-based supporting ligand activate O_2 through the formation of a *trans* μ-1,2-peroxo dinuclear Mn^{III} complex.[11b] This peroxo species directly evolves to a dinuclear μ-oxo Mn^{III} complex implicating the transient formation of oxo Mn^{IV} species.

In this context, we report here the unprecedented reactivity of a thiolate bound Mn^{II} complex with O_2 to yield *directly* high valent oxo Mn^{IV} species. As a precursor the reported dinuclear Mn^{II} complex $[Mn^{II}_2(LS)(LSH)]^+$ (**Mn^{II}_2SH**) (with LS^{2-} = 2,2′-(2,2′-bipyridine-6,6′-diyl)bis(1,1′-diphenylethanethiolate) was used, in which one thiol is terminally bound to a Mn^{II} ion.[12] This complex was previously shown to react with O_2 to generate a hydroxo bridged dinuclear Mn^{III} complex (**Mn^{III}_2OH**) (Scheme 1, top). In the present work, we provide evidence that the deprotonation of the Mn^{II}-bound thiol leads to the isolation of the first high-valent oxo Mn^{IV} dimer *directly* in a reaction with O_2 (Scheme 1, bottom). Finally,

a full mechanism of O_2 activation, starting either from **Mn^{II}_2SH** or from its deprotonated form **Mn^{II}_2**, is proposed based on experimental and computational studies. Especially, we demonstrate that that the oxo Mn^{IV} dimer is an intermediate species for the generation of **Mn^{III}_2OH** via comproportionation with the initial Mn^{II} species.

The thiol function of **Mn^{II}_2SH** can be deprotonated by addition of NaH (or 2,6-lutidine) to afford **Mn^{II}_2**. As expected, deprotonation induces a large decrease of the oxidation potential ($Mn^{II}Mn^{II}$ to $Mn^{III}Mn^{III}$) of the complex (of ~300 mV, see Figure S1).[12]

When O_2 is vigorously bubbled through a MeCN solution of **Mn^{II}_2**, the colour changes from light brown to black instantaneously with the appearance of a weak absorption band at 560 nm (Figure S2) that is assigned to the di–μ–oxo Mn^{IV} dimer, **$Mn^{IV}_2(O)_2$**. The conversion is quantitative based on the UV-vis spectrum of the oxygenated solution. Its structure, resolved by single crystal X-ray crystallography, displays a perfect planar $\{Mn_2O_2\}$ core with a C_2 symmetry axis passing through the two O atoms with each Mn in the center of a distorted N2S2O2 octahedron (Figure 1a). The Mn…Mn distance (2.7821(16) Å) and the Mn-O-Mn angles (100.5(2)° and 97.84(19)°) are consistent with a di–μ–oxo Mn^{IV} complex, where typical values in the range of 2.672–2.757 Å and 95.2–101.5° are found, respectively.[13]

X-ray absorption spectroscopy (XAS, Figure S3) and electrospray ionization (ESI)-mass spectrometry (Figures 2, S4, and S5) reveal the retention of the **$Mn^{IV}_2(O)_2$** structure in solution. The Mn K-edge absorption spectrum of **$Mn^{IV}_2(O)_2$** shows a shift to higher energy (6547.4 eV) of the Mn(1s) → Mn(4p) transition with respect to **Mn^{II}_2SH** and **Mn^{III}_2OH** (6545.5 and 6546.2 eV, respectively), as evidence of a +IV oxidation state for both Mn ions (Figure 3). The mass spectrum of a MeCN solution of **$Mn^{IV}_2(O)_2$** (m/z = 1299.4) indicates the presence of two additional oxygen atoms compared to the initial **Mn^{II}_2** complex (m/z = 1267.3). Furthermore, when **$Mn^{IV}_2(O)_2$** is generated in the presence of labeled $^{18}O_2$, only the **$Mn^{IV}_2(^{18}O)_2$** complex is observed in the mass spectrum (m/z = 1303.3). The present study unambiguously demonstrates that one molecule of O_2 reacts with **Mn^{II}_2** to form the two oxo-bridges in **$Mn^{IV}_2(O)_2$**. To the best of our knowledge, this is the first report on a Mn^{II} complex able to directly activate molecular oxygen to form a high-valent oxo-Mn^{IV} species.

The acid-base properties of **$Mn^{IV}_2(O)_2$** were investigated by UV-vis absorption spectroscopy in dimethylformamide solution at 273 K. In the presence of 1 equiv. of $HClO_4$, the 560 nm transition, characteristic for **$Mn^{IV}_2(O)_2$**, disappears with the concomitant apparition of two weak bands at 520 nm and 680 nm assigned to **$Mn^{IV}_2(O)(OH)$** (see Figure S2). The subsequent addition of 1 equiv. of a strong base (tBuOK) restores the initial UV-vis spectrum with a loss of about 10% of the intensity due to the slow decomposition of the complex in solution. Consistently no EPR transition could be observed in their respective spectra since an antiferromagnetic coupling between the two Mn^{IV} ions is expected resulting in a total spin $S = 0$ in both complexes.

The formed protonated species was assigned to a dinuclear μ–oxo-μ–hydroxo Mn^{IV} complex, **$Mn^{IV}_2(O)(OH)$**, based on the structure resolved by single crystal X-ray diffraction (Figure 1b). It represents the first crystallographically characterized μ-oxo-μ-hydroxo

dinuclear Mn^{IV} complex in the literature. Previously, Pecoraro et al. reported a series of di-μ-oxo, μ-oxo-μ-hydroxo, di-μ-hydroxo dinuclear Mn^{IV} complexes obtained with the salpn ligand (salpn=*N,N′*-bis(salicylidene)-1,3-diaminopropane). However, they only managed to structurally characterize these compounds by extended X-ray absorption fine structure (EXAFS) spectroscopy (except for the $[Mn^{IV}_2(salpn)_2(\mu\text{-}O)_2]$ complex).[14] The $\{Mn_2O_2\}$ core of **Mn^{IV}_2(O)(OH)** is planar as in **$Mn^{IV}_2(O)_2$**. In **Mn^{IV}_2(O)(OH)**, the two Mn sites are not equivalent anymore and each Mn centre has a distorted N2S2(O)(OH) octahedral geometry. In agreement with the presence of a hydroxo bridge, the Mn-O1(H) distance is about 10 pm longer (1.959(6) Å) than the Mn-O2 one (1.819(6) Å). Coherently, the Mn…Mn distance in **Mn^{IV}_2(O)(OH)** (2.922(2) Å) is longer than in **$Mn^{IV}_2(O)_2$** (2.7821(16) Å). The presence of the hydroxo bridge leads also to a smaller Mn1-O1(H)-Mn2 angle (96.1(3)°) with respect to the Mn1-O2-Mn2 one (107.2(3)°). The structural features of the Mn-O and Mn-O(H) bonds in **$Mn^{IV}_2(O)_2$** and **Mn^{IV}_2(O)(OH)** are similar to those found by Pecoraro et al.[14b] Subsequently, we evidenced that these high-valent oxo Mn^{IV} compounds are also involved as intermediates in the O_2 activation by the protonated **Mn^{II}_2SH** precursor. Firstly, we observed that this process can be directed towards either **Mn^{IV}_2(O)(OH)** or **Mn^{III}_2OH** by tuning the experimental conditions (relative concentration between the Mn^{II} precursor and O_2, protonation state of the Mn^{II} complex, temperature). Secondly, with the support of UV-vis absorption spectroscopy and ESI-mass spectrometry, we have made the following key observations: (i) even if both **Mn^{IV}_2(O)(OH)** and **$Mn^{IV}_2(O)_2$** decompose over time, none can directly evolve to **Mn^{III}_2OH** or to its deprotonated form **Mn^{III}_2O**, i.e. the μ-oxo Mn^{III} dimer,[15] (ii) **$Mn^{IV}_2(O)_2$** reacts instantaneously with **Mn^{II}_2SH** or **Mn^{II}_2** to generate **Mn^{III}_2OH** and/or **Mn^{III}_2O** *via* a comproportionation reaction, and (iii) the latter process is more efficient when the Mn^{II} precursor is protonated, i.e. **Mn^{II}_2SH**.

In the absence of available kinetic data (the oxygenation process is diffusion-limited), we have performed a DFT study to better understand the difference in reactivity between **Mn^{II}_2SH** and **Mn^{II}_2**. These exploratory calculations on the possible reaction cycles have been performed using previously benchmarked and calibrated methods for biomimetic manganese complexes.[16] The overall mechanism proposed for the reaction of **Mn^{II}_2SH** with O_2 is reported in Scheme 2 (see also Schemes S1 and S2) with a simplified representation of all calculated intermediate species. The activation of O_2 is proposed to go through the formation of a dinuclear *trans*-μ-1,2-peroxo Mn^{III} complex, **Mn^{III}_2(OO)SH**, whose calculated structural parameters are comparable to those reported for the similar complex described by Kovacs et al.[11b] This *trans*-μ-1,2-peroxo Mn^{III} complex converts to a dinuclear di-μ-oxo Mn^{IV} species with large exothermicity (of −41.5 kcal mol^{-1}), and a low transition state (**TS_{OO}**) with a barrier of only 5.8 kcal mol^{-1}. The rupture of the O-O bond leads to a rapid internal proton transfer from the thiol to one of the bridging oxygen atoms via a proton transfer barrier (**TS_{PT}**) of about 11.5 kcal mol^{-1} and the formation of the experimentally characterized **Mn^{IV}_2(O)(OH)** complex. Then a comproportionation reaction with a molecule of **Mn^{II}_2SH** can occur to form the dinuclear μ-hydroxo Mn^{III} product, **Mn^{III}_2OH**, with large exothermicity (−56.0 kcal mol^{-1}). As each individual step in the reaction mechanism of Scheme 2 is exothermic, this implies that the reaction is irreversible and the final products will be the most stable. As a matter of fact, most of these structures could be characterized experimentally, hence validating our proposed mechanism.

We have also calculated the mechanism of O_2 activation starting from the deprotonated **Mn^{II}_2** complex (Scheme S2 and Figure S6). It is found that the process is energetically less favorable than the one starting from the **Mn^{II}_2SH** complex, but still feasible. From these different pathways, it can be concluded that the formation of either a dinuclear Mn^{III} or Mn^{IV} complex will depend on the relative rates between the O_2 activation processes (steps 1–2 in Scheme 2, formation of **Mn^{III}_2(OO)SH**) and the comproportionation reaction (step 5 in Scheme 2). In the case of a faster O_2 activation, the initial Mn^{II} complex will be entirely consumed to form the Mn^{IV} derivate and thus the Mn^{III} dimer cannot be generated. Conversely, in the case of a faster comproportionation reaction, a part of the Mn^{II} complex will remain unreacted to O_2, and will thus combine with the generated Mn^{IV} species to yield the Mn^{III} dimer. This is consistent with the fact that a higher concentration of O_2 vs. Mn^{II} complex promotes the formation of the Mn^{IV} compound as final product instead of **Mn^{III}_2OH**.

Based on these considerations, two complementary reasons can explain how protonation of the Mn^{II} precursor favors the production of the Mn^{III} complex to the detriment of the Mn^{IV} one: (i) O_2 activation is expected to be slower in the case of **Mn^{II}_2SH** (higher $Mn_2^{II,II}$/$Mn_2^{III,III}$ anodic potential compared to **Mn^{II}_2**) and (ii) the comproportionation reaction is more efficient when protonated species are involved, as shown experimentally (see above) and corroborated by DFT.

The calculated mechanism reveals a short-lived *trans* μ-1,2 peroxo Mn^{III} complex as a key intermediate in the formation of high valent oxo/hydroxo Mn^{III} and Mn^{IV} dimers from the reaction of the Mn^{II} complexes with O_2 (Table S23). As noted previously, a similar peroxo complex has been isolated by the Kovacs group through the reaction of a Mn^{II} thiolate complex ($[Mn(L^{N4S})]^+$) with O_2, and characterized by single crystal X-ray diffraction (Scheme S3). This complex slowly evolves into a dinuclear μ-oxo Mn^{III} complex (Eqs 1 and 2).[11b]

$$2\,[\mathrm{Mn}(\mathrm{L}^{\mathrm{N4S}})]^{+} + \mathrm{O}_2 \rightarrow [\,(\mathrm{L}^{\mathrm{N4S}})\mathrm{MnOOMn}(\mathrm{L}^{\mathrm{N4S}})]^{2+} \quad \text{Eq. 1}$$

$$2[\,(\mathrm{L}^{\mathrm{N4S}})\mathrm{MnOOMn}(\mathrm{L}^{\mathrm{N4S}})]^{2+} \rightarrow 2[\,(\mathrm{L}^{\mathrm{N4S}})\mathrm{MnOMn}(\mathrm{L}^{\mathrm{N4S}})]^{2+} + \mathrm{O}_2 \quad \text{Eq. 2}$$

Although **Mn^{II}_2** (or **Mn^{II}_2SH**) and $[Mn(L^{N4S})]^+$ complexes contain a thiolate-based ligand, their reactivity patterns are significantly different. First, in the Kovacs' system the peroxo Mn^{III} species is the most stable intermediate, while in our case it is the di-μ-oxo Mn^{IV} species (the peroxo intermediate is too reactive to be trapped). Secondly, to form the dinuclear μ-oxo Mn^{III} complex, a comproportionation reaction is required with the LS^{2-} system, while the Kovacs' peroxo, $[(L^{N4S})MnOOMn(L^{N4S})]^{2+}$, evolves directly into the $[(L^{N4S})MnOMn(L^{N4S})]^{2+}$ species (Eq. 2).

In principle, this “direct” pathway should also be considered for **Mn^{III}_2(OO)SH**, but this reaction does not occur as observed experimentally in solution. Although the hypothetical dissociation of two **Mn^{III}_2(OO)SH** complexes into two **Mn^{III}_2OH** complexes and O_2 (as in Eq. 2) should be preferred under thermodynamic control (the calculated energy gap of −64.6 kcal mol^{-1} is larger than that between **Mn^{III}_2(OO)SH** and **Mn^{IV}_2(O)$_2$SH**, which is of −41.5 kcal mol^{-1}), the lifetime of **Mn^{III}_2(OO)SH** is too short to allow the reaction with a second **Mn^{III}_2(OO)SH** molecule and the peroxo species more readily evolves into **Mn^{IV}_2(O)(OH)**. Such difference in reactivity between our system and the one of Kovacs et al. is consistent with the fact that the O-O bond is longer in the calculated structure of **Mn^{III}_2(OO)SH** than in $[(L^{N4S})MnOOMn(L^{N4S})]^{2+}$ (1.488 Å vs 1.452 Å, respectively). Indeed DFT shows that the O-O bond is more easily cleaved in **Mn^{III}_2(OO)SH**. The lower stability of **Mn^{III}_2(OO)SH** compared to $[(L^{N4S})MnOOMn(L^{N4S})]^{2+}$ may be also rationalized in terms of differences in metal coordination sphere. First, the N2S2 ligand leads to a peroxo dimer with an unfavorable 5-coordinated geometry for a Jahn-Teller Mn^{III} ion, while a stable peroxo Mn^{III} dimer with a suited 6-coordinated geometry is obtained with the L^{N4S} ligand. Secondly, the O-O bond cleavage of **Mn^{III}_2(OO)SH** yields a stable 6-coordinated di-μ-oxo Mn^{IV} species, while formation of a similar species with the L^{N4S} ligand features is unlikely since it should involve the formation of a 7-coordinated Mn^{IV} complex or the decoordination of a N-based donor atom. Although the reactivity of these two thiolate-based Mn^{II} complexes differs significantly, the role of the metal-bound thiolate to promote O_2 activation is, however, once more highlighted.

In summary, our work reports the unprecedented reactivity of a non heme Mn^{II} complex towards O_2. We showed that, by conveniently tuning the experimental conditions (room temperature, ligand deprotonation, low precursor concentration and high O_2 concentration), the process can be directed to fully-characterized high-valent μ-oxo and μ-hydroxo-μ-oxo Mn^{IV} dimers.

Supplementary Material

Refer to Web version on PubMed Central for supplementary material.

Acknowledgments

The authors gratefully acknowledge research support of this work by the French National Agency for Research (no. ANR- 09-JCJC-0087), Labex arcane (ANR-11-LABX-003) and COST Action (CM1305 ECOSTBio, Explicit Control Over Spin-States in Technology and Biochemistry) especially *via* STSM 34962. FGCR and ASF thank the Conacyt Mexico and the Tertiary Education Trust Fund Nigeria for studentships, respectively. XAS studies at SSRL BL 9-3 were made possible by the US DOE Office of Science (Contract No. DE-AC02-76SF00515) and US NIH (P41-GM-103393 to SSRL SMB Program and P30-EB-009998 to CWRU Center for Synchrotron Biosciences. We thank Dr. E. W. Farquhar for collection of data.

References

1. a) Simandi, LI. Catal Met Complexes. Kluwer Academic Publishers; 2003. Advances in Catalytic Activation of Dioxygen by Metal Complexes; p. 26b) Kaila VRI, Verkhovsky MI, Wikstrom M. Chem Rev. 2010; 110:7062–7081. [PubMed: 21053971] c) Tolman WB, Solomon EI. Inorg Chem. 2010; 49:3555–3556. [PubMed: 20380456] d) Hematian S, Garcia-Bosch I, Karlin KD. Acc Chem Res. 2015; 48:2462–2474. [PubMed: 26244814]
2. Shilov AE, Shul’pin GB. Chem Rev. 1997; 97:2879–2932. [PubMed: 11851481]

3. a) Adler SB. Chem Rev. 2004; 104:4791–4843. [PubMed: 15669169] b) Shao M, Chang Q, Dodelet JP, Chenitz R. Chem Rev. 2016; 116:3594–3657. [PubMed: 26886420]
4. a) Yee, GM., Tolman, WB. Sustaining Life on Planet Earth: Metalloenzymes Mastering Dioxygen and Other Chewy Gases. Kroneck, PMH., Sosa Torres, ME., editors. Springer International Publishing; Cham: 2015. p. 131-204.b) Fiedler AT, Fischer AA. J Biol Inorg Chem. 2016; doi: 10.1007/s00775-00016-01402-00777
5. a) Fukuzumi S, Okamoto K, Gros CP, Guilard R. J Am Chem Soc. 2004; 126:10441–10449. [PubMed: 15315460] b) Halime Z, Kotani H, Li Y, Fukuzumi S, Karlin KD. Proc Natl Acad Sci U S A. 2011; 108:13990–13994. [PubMed: 21808032] c) Tahsini L, Kotani H, Lee YM, Cho J, Nam W, Karlin KD, Fukuzumi S. Chem Eur J. 2012; 18:1084–1093. [PubMed: 22237962] d) Ray K, Pfaff FF, Wang B, Nam W. J Am Chem Soc. 2014; 136:13942–13958. [PubMed: 25215462] e) Rosenthal J, Nocera DG. Acc Chem Res. 2007; 40:543–553. [PubMed: 17595052] f) Costas M, Mehn MP, Jensen MP, Que L Jr. Chem Rev. 2004; 104:939–986. [PubMed: 14871146] g) Peljo P, Murtomaki L, Kallio T, Xu HJ, Meyer M, Gros CP, Barbe JM, Girault HH, Laasonen K, Kontturi K. J Am Chem Soc. 2012; 134:5974–5984. [PubMed: 22420745]
6. a) Solomon EI, Goudarzi S, Sutherlin KD. Biochemistry. 2016; 55:6363–6374. [PubMed: 27792301] b) Nam W. Acc Chem Res. 2015; 48:2415–2423. [PubMed: 26203519] c) McDonald AR, Que L Jr. Coord Chem Rev. 2013; 257:414–428.
7. a) Solomon EI. Inorg Chem. 2016; 55:6364–6375. [PubMed: 27299802] b) Quist DA, Diaz DE, Liu JJ, Karlin KD. J Biol Inorg Chem. 2017; 22:253–288. [PubMed: 27921179] c) Keown W, Gary JB, Stack TDP. J Biol Inorg Chem. 2017; 22:289–306. [PubMed: 27909921] d) McCann SD, Stahl SS. Acc Chem Res. 2015; 48:1756–1766. [PubMed: 26020118] e) Elwell CE, Gagnon NL, Neisen BD, Dhar D, Spaeth AD, Yee GM, Tolman WB. Chem Rev. 2017; 117:2059–2107. [PubMed: 28103018]
8. Sahu S, Goldberg DP. J Am Chem Soc. 2016; 138:11410–11428. [PubMed: 27576170]
9. Engelmann X, Monte-Pérez I, Ray K. Angew Chem Int Ed. 2016; 55:7632–7649.
10. Parsell TH, Behan RK, Green MT, Hendrich MP, Borovik AS. J Am Chem Soc. 2006; 128:8728–8729. [PubMed: 16819856]
11. a) Deville C, Padamati SK, Sundberg J, McKee V, Browne WR, McKenzie CJ. Angew Chem Int Ed. 2016; 55:545–549.b) Coggins MK, Sun X, Kwak Y, Solomon EI, Rybak-Akimova EV, Kovacs JA. J Am Chem Soc. 2013; 135:5631–5640. [PubMed: 23470101]
12. Gennari M, Brazzolotto D, Pecaut J, Cherrier MV, Pollock CJ, DeBeer S, Retegan M, Pantazis DA, Neese F, Rouzieres M, Clerac R, Duboc C. J Am Chem Soc. 2015; 137:8644–8653. [PubMed: 26076066]
13. Mukhopadhyay S, Mandal SK, Bhaduri S, Armstrong WH. Chem Rev. 2004; 104:3981–4026. [PubMed: 15352784]
14. a) Baldwin MJ, Stemmler TL, Riggs-Gelasco PJ, Kirk ML, Penner-Hahn JE, Pecoraro VL. J Am Chem Soc. 1994; 116:11349–11356.b) Krewald V, Lassalle-Kaiser B, Boron TT, Pollock CJ, Kern J, Beckwith MA, Yachandra VK, Pecoraro VL, Yano J, Neese F, DeBeer S. Inorg Chem. 2013; 52:12904–12914. [PubMed: 24161030]
15. $Mn^{III}_2(OH)$ and $Mn^{III}_2(OH)$ cannot be distinguished by UV-visible spectroscopy since both spectra are dominated by one intense thiolate to Mn^{III} charge transfer feature.
16. a) Yang T, Quesne MG, Neu HM, Cantú Reinhard FG, Goldberg DP, de Visser SP. J Am Chem Soc. 2016; 138:12375–12386. [PubMed: 27545752] b) Barman P, Upadhyay P, Faponle AS, Kumar J, Nag SS, Kumar D, Sastri CV, de Visser SP. Angew Chem Int Ed. 2016; 55:11091–11095.

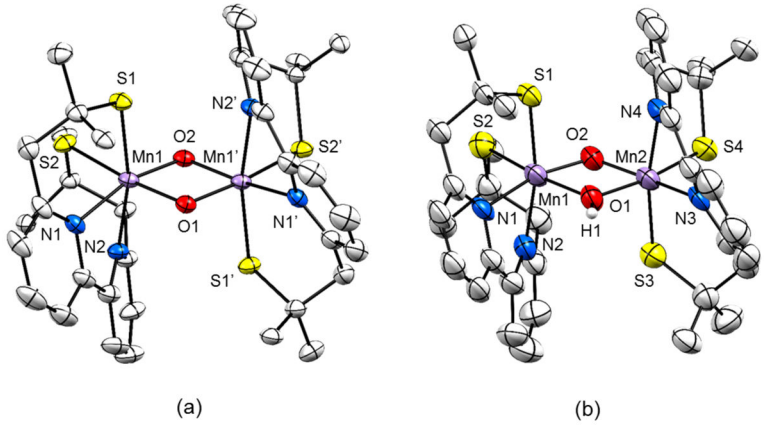

Figure 1.

Molecular structures of (a) $\mathbf{Mn^{IV}_2(O)_2}$·1.34CH_2Cl_2.5.82H_2O and (b) $\mathbf{Mn^{IV}_2(O)(OH)}$$ClO_4$.5.68$CH_3CN$.1.5$H_2O$. The thermal ellipsoids are drawn at 50% probability level. For clarity, phenyl groups, all hydrogen atoms (except for H1 in b), anions and solvent molecules are omitted. Selected bond distances (Å): in $\mathbf{Mn^{IV}_2(O)_2}$, Mn1-O1 = 1.845(3), Mn1-O2 = 1.809(3), Mn1-Mn1′ = 2.7821(16); in $\mathbf{Mn^{IV}_2(O)(OH)}$, Mn1-O1 = 1.959(6), Mn1-O2 = 1.819(6), Mn1-Mn1′ = 2.922(2).

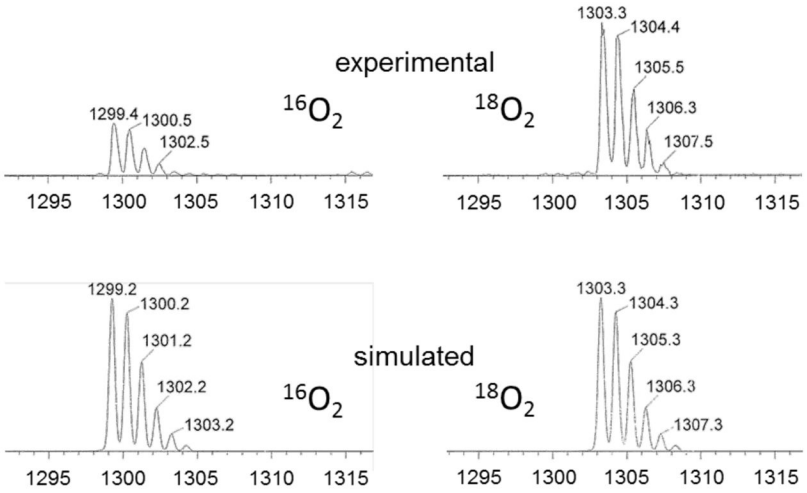

Figure 2.

Experimental and simulated ESI-mass spectra of $\mathbf{Mn^{IV}_2(O)_2}$ generated from $\mathbf{Mn^{II}_2}$ and either $^{16}O_2$ or $^{18}O_2$.

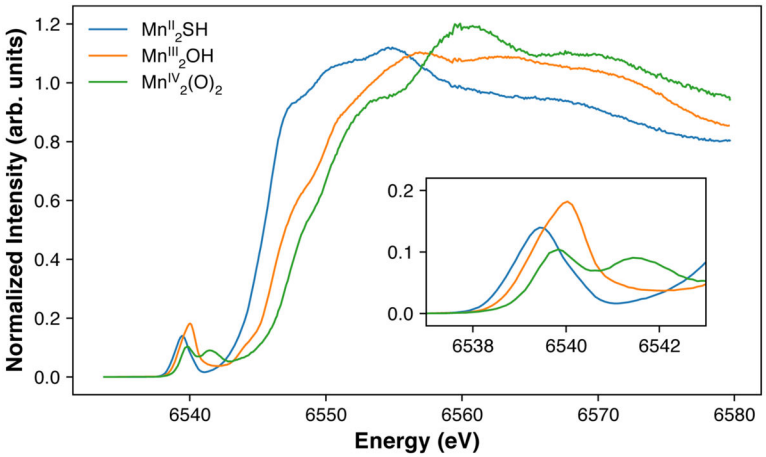

Figure 3.

(a) Mn K-edge XAS spectra recorded on powdered samples of **Mn^{II}_2**, **Mn^{III}_2 OH**, and **$Mn^{IV}_2(O)_2$**. The pre-edge region is shown in the inset.

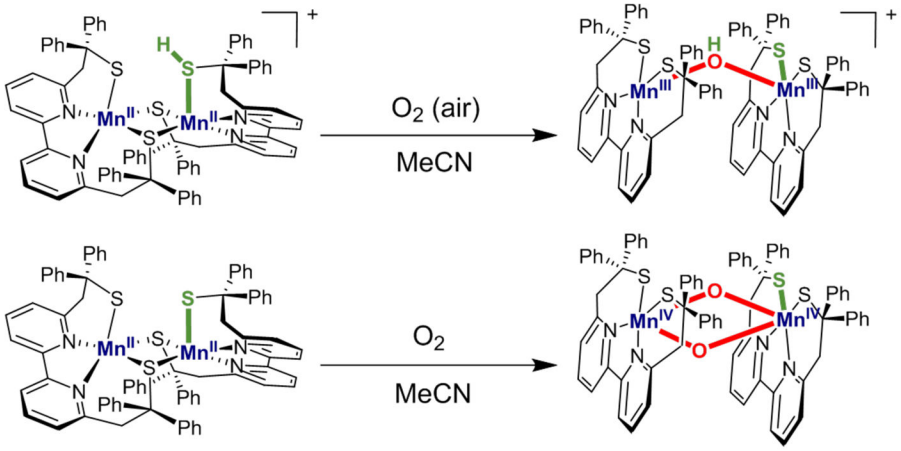

Scheme 1.

Reaction of $\mathbf{Mn^{II}_2SH}$ (top) and $\mathbf{Mn^{II}_2}$ (down) with O_2 in MeCN at 293 K.

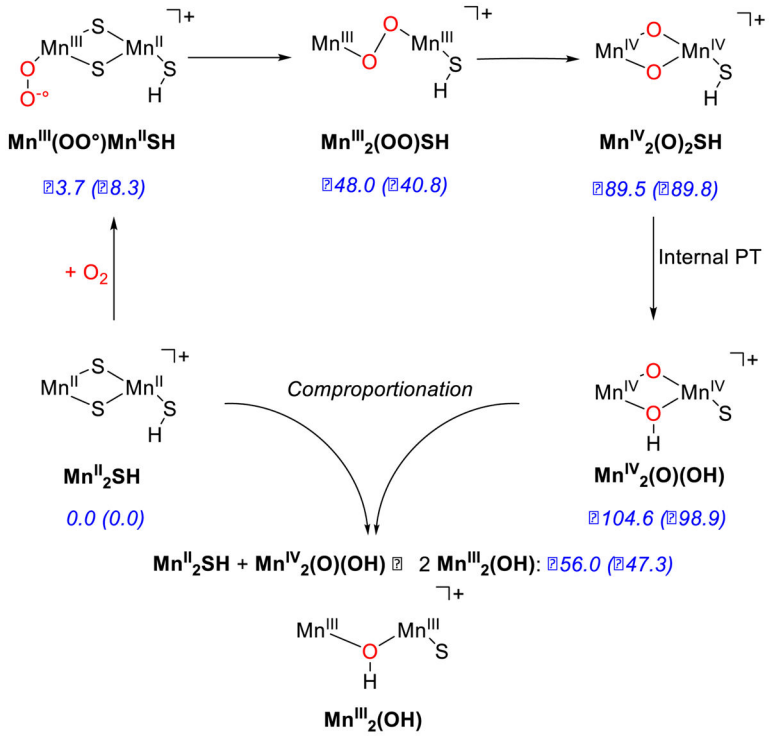

Scheme 2.

Dioxygen activation mechanism on **Mn^{II}_2SH** as calculated using DFT at the BLYP/BS2//BLYP/BS1 level of theory. Relative energies of the antiferromagnetic spin states for the pathway leading to the $Mn^{IV}_2(O)(OH)$ complex are in kcal mol^{-1} with respect to **Mn^{II}_2SH** + O_2 and contain zero-point energy and solvent corrections. Data out of parenthesis represent the full model and inside parenthesis the small model with methyl rather than phenyl substituents on the N2S2 ligand. Also given are the energetics for the comproportionation reaction.